Materials Today Bio 20 (2023) 100684

Contents lists available at ScienceDirect

Materials Today Bio

journal homepage: www.journals.elsevier.com/materials-today-bio

Immunosuppressive dead cell as lung-targeting vehicle and cytokine absorption material for cytokine storm attenuation of pneumonia

Tianyuan Ci [1,*], Yaoxuan Xiong [1], Jinniu Zhang, Jing Zang, Nianping Feng [**]

School of Pharmacy, Shanghai University of Traditional Chinese Medicine, Shanghai, 201203, China

ARTICLE INFO

Keywords:
Dead cell
Pneumonia
Immunosuppression
Lung targeting
Cytokine storm

ABSTRACT

Effectively controlling cytokine storm is important to reduce the mortality of severe pneumonia. In this work a bio-functional dead cell was engineered by one-time quick shock of live immune cells in liquid nitrogen, and the obtained immunosuppressive dead cell could server as both lung-targeting vehicle and cytokine absorption material. After loading the anti-inflammatory drugs of dexamethasone (DEX) and baicalin (BAI), the drug-loaded dead cell (DEX&BAI/Dead cell) could first passively target to the lung after intravenous administration and quickly release the drugs under high shearing stress of pulmonary capillaries, realizing drug enrichment in the lung. Then, the immunosuppressive dead cell acted as the camouflage of normal immune cells with various cytokine receptors exposing on their surface, to "capture" the cytokines and further reduce the state of inflammation. With above formulation design, a synergic anti-inflammatory effect between drugs and carrier could be achieved. In a lipopolysaccharide-induced pneumonia mice model, this system could calm down the cytokine storm with high efficacy and elongate the survival of mice.

1. Introduction

Pneumonia is a widespread infection disease of respiratory system, which is generally caused by the invasion of bacteria or virus, causing inflammation in the lung tissue [1,2]. When the invaded pathogens are numerous or severe, these exogenous substances will lead to imbalance of immune homeostasis with over-activation of immune cells and excessive production of various cytokine [3–5]. Cytokine storm is considered as the main lethal factor of severe pneumonia [6–8], and efficient inhibition of uncontrolled inflammatory responses and reducing the level of inflammatory cytokines are important to control severe pneumonia and reduce mortality.

Clinical strategies of attenuating cytokine storm include immunosuppressive drugs such as glucocorticoids [9,10], or neutralizing antibody such as Tocilizumab [11,12]. However, above two schemes still have some limitations in practical applications. The use of high dosage of corticosteroids may lead to serious adverse reactions, such as osteonecrosis of the femoral head [13–15]. And single neutralizing antibody treatment may have limited anti-inflammation efficacy, regarding the cytokine storm is usually the results of various inflammatory factors [16].

Immune cells play an important role in mediating the occurrence and development of cytokine storm [17–19]. For example, the macrophages in the lung can recognize the exogenous stimuli at the first time and recruit neutrophils in blood circulation by secreting cytokines to enhance immune response [20,21]. Our previous work engineered functional dead cells *via* treating the live cell by one-time quick shocking with liquid nitrogen [22]. The obtained cells lost proliferation capability but maintained the cellular structure and protein-related bioactivities. Thus, we designed the immunosuppressive dead cells with similar strategy by shocking the immune cells with liquid nitrogen, and utilized this kind of dead cell as delivery vehicles of the anti-inflammatory drugs of dexamethasone (DEX) and baicalin (BAI).

In this system, the immunosuppressive dead cell first acted as the lung targeting vehicle due to its cellular size and quickly released the loaded anti-inflammatory drugs in the lung, then behaved as "mixed antibodies" of inflammatory cytokines to further decrease the cytokine levels (Fig. 1). The drugs and immunosuppressive dead cells worked synergistically to calm down the cytokine storm of severe pneumonia.

* Corresponding author.
** Corresponding author.
E-mail addresses: tianyuanci@shutcm.edu.cn (T. Ci), npfeng@shutcm.edu.cn (N. Feng).
[1] These authors contributed equally to this work.

https://doi.org/10.1016/j.mtbio.2023.100684
Received 8 February 2023; Received in revised form 26 May 2023; Accepted 26 May 2023
Available online 27 May 2023

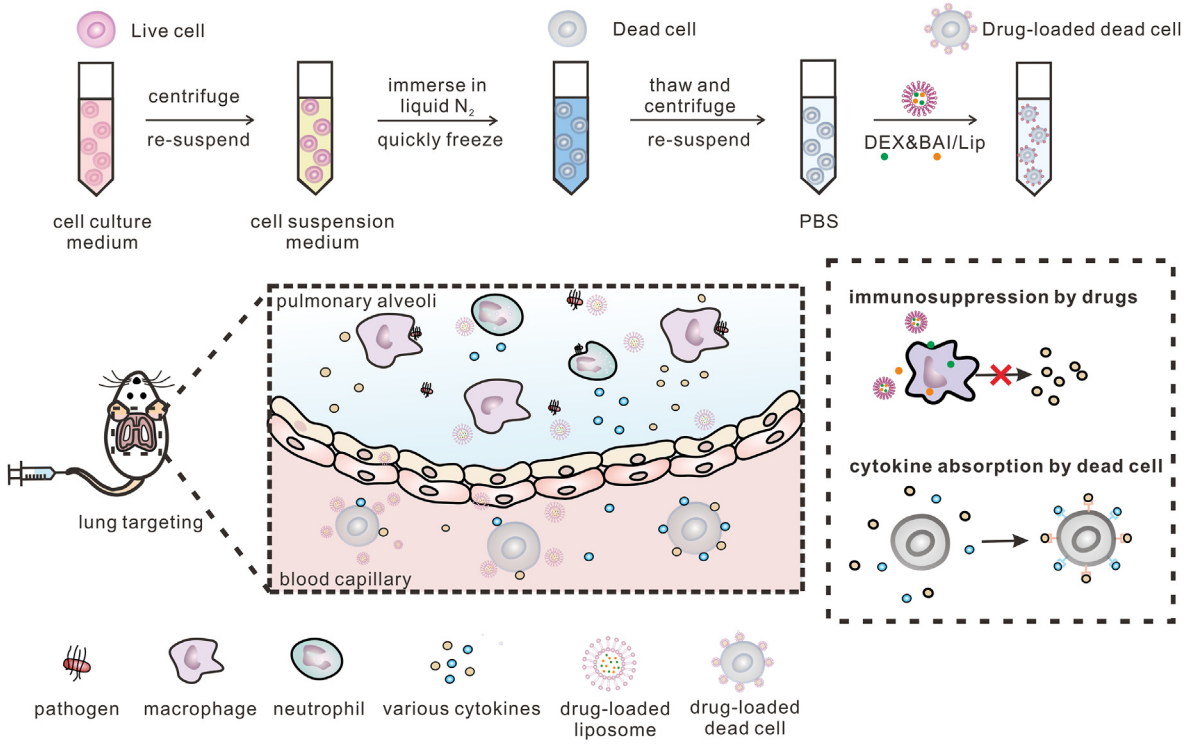

Fig. 1. Preparation scheme of the drug-loaded immunosuppressive dead cell and the *in vivo* anti-inflammation mechanisms.

2. Materials and methods

2.1. Materials

Dexamethasone (DEX), baicalin (BAI), lecithin, cholesterol, octadecylamine were bought from Aladdin Corporation (Shanghai, China). Lipopolysaccharide (LPS) was provided by Shanghai Yuanye Biotechnology Co., Ltd (Shanghai, China). The enzyme-linked immunosorbent assay (Elisa) kits (IL-6, TNF-α, IL-1β, CXCL2) and fluorescence-labelled antibodies (APC-CXCR2, APC-TLR4, PE-CD121a, PE-gp130, PE-CD120a, PE-CD14, PE-F4/80, APC-CD11b, PE-Ly6G) were purchased from Biolegend Corporation (California, USA). Rhodamine labelled phalloidin (Rhodamine-Phalloidin) was purchased from Suzhou UElandy Biotechnology Co., Ltd (Suzhou, China). Hoechst 33,342, dulbecco's modified eagle medium (DMEM) and dimethylsulfoxide (DMSO) were provided by Jiangsu Kaiji Biotechnology Co., Ltd (Jiangsu, China). Calcein/PI cell viability kit was purchased from Beyotime Biotechnology Co., Lt (Shanghai, China). Cell counting kit-8 (CCK-8) was provided by Dalian Meilun Biotechnology Co., Ltd (Dalian, China). The murine mononuclear macrophage cell line J774A.1 and fetal bovine serum (FBS) were purchased from Shanghai Fuheng Biotechnology Co., Ltd (Shanghai, China). Balb/c female mice were supplied by Animal Experimental Center of Shanghai University of Traditional Chinese Medicine. All animal tests complied with the animal protocol approved by the institutional animal care and use committee of Shanghai University of Traditional Chinese Medicine (PZSHUTCM211213020).

2.2. Cell culture

J774A.1 were cultured in the cell incubator (37 °C, 5% CO_2) with the culture medium of DMEM supplemented with 10% FBS and 1% penicillin streptomycin. The cells were passed after reaching 70–80% confluence.

2.3. Preparation of J774A.1 dead cell

Live J774A.1 cells were suspended in a cell suspension medium (75% DMEM, 20% FBS, 5% DMSO) and quickly immersed in liquid nitrogen overnight. Before use, the frozen cells were thawed at 37 °C and washed with phosphate buffered saline (PBS). After centrifuging at 200 g for 5 min, the dead cells were obtained.

2.4. Characterization of J774A.1 dead cell

The cellular structure of the dead cell was analyzed by confocal laser microcopy after fluorescence staining. 1×10^6 J774A.1 dead cells were suspended in 200 μl PBS and 5 μl Rhodamine-Phalloidin stock solution was added to stain the cells at room temperature for 20 min. After that, the cells were centrifuged at 200 g for 5 min and washed with PBS. The cells were resuspended in 1 ml Hoechst 33,342 staining solution and stained for 10 min. After washing with PBS, the cells were suspended in 100 μl PBS and observed by laser confocal microscope. Live J774A.1 cells were first seeded into confocal dishes and washed with PBS before use. After fixing with 4% paraformaldehyde, 0.1% Triton X-100 solution was added to destroy the cell membrane. After washing with PBS twice, the cells were stained with Rhodamine-Phalloidin and Hoechst 33,342 similar as the dead cells. For cell viability analysis, the cells were stained with Calcein/PI kit according to the manufacturer's protocol. After staining by calcein AM and PI, the cells were analyzed by confocal microscopy. For scanning electron microscopy (SEM) characterization, both J774A.1 dead cells and live cells were fixed with 2.5% glutaraldehyde solution at 4 °C for 12 h. Then the cells were further treated with 1% osmic acid for 2 h. After washing with PBS three times, the cells were treated with different concentrations of ethanol for gradient dehydration (30%, 50%, 70%, 80%, 90% once, 15 min each time, 100% twice, 20 min each time) and dropped on silica plates. After drying and gold spraying, the samples were photographed by SEM.

2.5. In vitro proliferation of dead cell

J774A.1 dead cells were suspended in the cell culture medium (90% DMEM, 10% FBS) and seeded into 96-well plate with a cell density of 5×10^3 cells per well. After 0.5 h, 24 h, 48 h and 72 h, 10 μl CCK-8 solution

was added to each well and further incubate the cells for 2.5 h. The absorbance was measured at 450 nm with the microplate reader.

2.6. Cytokine secretion of the dead cells

J774A.1 dead cells were seeded in 24-well plate (1×10^5 per well) and stimulated with LPS (50 ng ml^{-1}). 8 h later, the supernatant of the cell culture medium was collected and centrifugated at 300 g for 10 min. The cytokine levels of IL-6, TNF-α and CXCL2 were detected by ELISA kits. In comparison, the cytokine secretion of live J774A.1 cells after LPS stimulation was set as positive control, while J774A.1 dead cells without LPS stimulation as the negative control.

2.7. Biosafety evaluation of the dead cell

Healthy Balb/c female mice were randomly divided into saline group and dead cell group (2×10^6). After intravenous injection, the survival of mice was recorded.

The biosafety of J774A.1 dead cells was also evaluated in pneumonia-model mice. The model was established by intratracheal instillation of LPS (10 mg kg^{-1}). After 4 h, saline, dead cells (2×10^6), live cells (2×10^6) were intravenously injected, respectively. 24 h later, the blood was collected from the eyeballs of mice. After centrifuging at 3000 rpm for 10 min, the levels of serum cytokines were measured by ELISA kits. Meanwhile, the survival of mice was recorded.

2.8. Screening of drug combination proportion

First, the anti-inflammatory effects of DEX and BAI were investigated by evaluation of the cytokine secretion of J774A.1 cells after stimulation by LPS. In brief, live J774A.1 cells were seeded in a 24-well plate (1×10^5 per well) and cultured overnight. LPS (50 ng ml^{-1}) was added in the culture medium to stimulate the cells for 2 h. Then DEX solutions (0.5,1,5,10 μM) or BAI solutions (6.25, 12.5, 25, 50 μM) were added in the well. After further incubating the cells for 8 h, the supernatant of the culture medium in each well was collected and IL-6 concentration was determined by ELISA kit. Second, half inhibitory concentration (IC_{50}) of DEX ($IC_{50,\ DEX}$) and BAI ($IC_{50,\ BAI}$) were calculated by the software Compusyn. The combination ratios were set as: 100% $IC_{50,\ DEX}$, 95% $IC_{50,\ DEX}$ + 5% $IC_{50,\ BAI}$ (19:1), 93.33% $IC_{50,\ DEX}$ + 6.67% $IC_{50,\ BAI}$ (14:1), 90% $IC_{50,\ DEX}$ + 10% $IC_{50,\ BAI}$ (9:1), 80% $IC_{50,\ DEX}$ + 20% $IC_{50,\ BAI}$ (4:1), 50% $IC_{50,\ DEX}$ + 50% $IC_{50,\ BAI}$ (1:1), 20% $IC_{50,\ DEX}$ + 80% $IC_{50,\ BAI}$ (1:4), 10% $IC_{50,\ DEX}$ + 90% $IC_{50,\ BAI}$ (1:9), 6.67% $IC_{50,\ DEX}$ + 93.33% $IC_{50,\ BAI}$ (1:14), 5% $IC_{50,\ DEX}$ + 95% $IC_{50,\ BAI}$ (1:19) and 100% $IC_{50,\ BAI}$. Determine IL-6 levels of different groups with similar procedure described above to investigate the synergetic anti-inflammatory effects of the two drugs.

2.9. Preparation and characterization of drug-loaded dead cell

The drug loading process included two typical procedures, preparation of DEX&BAI/liposomes (DEX&BAI/Lip) and the incubation of DEX&BAI/Lip with J774A.1 dead cells. The drugs could be loaded *via* the electrostatic interactions between cationic liposomes and dead cells. The liposomes were prepared by thin-film hydration method. In brief, 19.8 mg lecithin, 6 mg cholesterol, 1.65 mg DEX, 1.65 mg BAI and 3 mg octadecylamine were added in the round-bottom bottle and dissolved by 12 ml mixed solvent of chloroform and methanol (chloroform: methanol = 1:2, V/V). The sample was vacuumized with a rotary evaporator (rotational speed of 60 rpm, 25 °C) until a uniform film was formed. After hydration with 6 ml PBS for 2 h, the solution was conducted ultrasonication for 15 min (40 Hz probe) and passed through 0.45 μm and 0.22 μm filter to obtain DEX&BAI/Lip. The obtained DEX&BAI/Lip were further incubated with 1×10^6 J774A.1 dead cells for 1 h. After 200 g centrifugation for 5 min, the drug-loaded dead cells (DEX&BAI/Dead cell) were obtained. For drug loading analysis, the loaded drugs were extracted with 500 μl methanol and ultrasound for 15 min. After centrifuging at 12,000 rpm for 10 min, the supernatant was analyzed by HPLC to determine the drug content. To visualize the drug loading state in dead cells, coumarin 6 (Cou-6) was adopted as the model drug. The preparation procedure of Cou-6/Dead cell was similar as stated above and Cou-6/Dead cell was observed by laser confocal microscope.

2.10. In vitro drug release of drug-loaded dead cells

DEX&BAI/Lip was added to the dialysis bag (molecular interception 3500 Da), and immersed in a dissolution cup containing 80 ml PBS (37 °C, 100 r min^{-1}). 2 ml PBS was collected from the dissolution cup at 10 min, 20 min, 30 min, 1 h, 2 h, 4 h, 8 h and 12 h, respectively. The concentrations of dexamethasone and baicalin in the sample were determined by HPLC.

The drug shedding behavior from dead cells was evaluated with a peristaltic pump to mimic the *in vivo* blood flow. In brief, the initial fluorescence intensity of Cou-6/Dead cell was determined and recorded. After starting the peristaltic pump (shearing force of 0 Pa, 2 Pa, 6 Pa), the fluorescence intensity of each time (10 min, 30 min, 60 min and 90 min) of the circulating medium (4 ml PBS) was detected after filtration with 0.8 μm filter, each set of data is repeated three times. The unreleased drug percentage was calculated by the equation: remaining fluorescence intensity/initial fluorescence intensity × 100%.

2.11. Protein expression of J774A.1 dead cells

The protein expression of J774A.1 dead cells was evaluated by immunofluorescent staining. The dead cells were suspended in 500 μl PBS (1% FBS) and stained with fluorescence-labelled antibodies (APC-CXCR2, APC-TLR4, PE-CD121a, PE-gp130, PE-CD120a and PE-CD14) for 30 min. After incubation, 10 ml PBS (1% FBS) was added to and centrifuge at 250 g for 5 min twice. Then 400 μl PBS (1% FBS) was added to resuspend the cells and further the cells were analyzed by laser confocal microscope and flow cytometry. The live J774A.1 cells were treated similar as dead cells after scraping the cells with cell scraper.

2.12. Absorption of cytokines by J774A.1 dead cells

10 μl FAM-NHS solution (10 ng ml^{-1}) was added to 250 μl IL-6 solution (10.4 ng ml^{-1}) and incubated at 4 °C for 8 h. Free FAM was removed by 12,000 rpm centrifugation for 10 min with 3 KD ultrafiltration tube and washed with 300 μl PBS for 3 times. Then the dead cells were incubated in fluorescent labelled IL-6 solution for 1 h and washed with PBS. The dead cells were re-suspended in PBS and observed by laser confocal microscope.

IL-6 standard solution (250 pg ml^{-1}) was incubated with dead cells (2×10^6 cells) and added in 96-well plate. 2 h later, the supernatant was collected after centrifugation and the concentration of IL-6 was detected by Elisa kit, and the untreated IL-6 standard solution (without dead cell incubation) was used as negative control.

2.13. In vitro immunosuppression of dead cells and drug-loaded dead cells

DC 2.4 cells were seeded in 6-well plates (1×10^6 cells per well). After culturing for overnight, saline, LPS (50 ng ml^{-1}) and LPS + dead cells (50 ng ml^{-1}, dead cell 1×10^6 cells per well) were added respectively. After 24 h, DC 2.4 cells were collected and stained with FITC-CD11c, APC-CD86 and PE-CD80 for 1 h. The cells were further analyzed by flow cytometry.

The mononuclear macrophage J774A.1 were seeded into 24-well plate with the cell density of 1×10^5 cells per well and cultured for 12 h. LPS (50 ng ml^{-1}) was added into each well to activate the cells for 2 h. Then different groups of saline, dead cell (1×10^5 cells per well) was added to each well and incubate for further 2 h, 6 h, 10 h, 22 h. The cell supernatant was collected at different time points, the cytokine levels of IL-6 were detected by ELISA kits.

The mononuclear macrophage J774A.1 were seeded into 24-well plate with the cell density of 1×10^5 cells per well and cultured for 12 h. LPS (50 ng ml^{-1}) was added into each well to stimulate J774A.1 cells for 2 h. Then different groups of saline, dead cell (1×10^5 cells per well) and drug-loaded dead cell (1×10^5 cells per well, DEX 16.41 μg ml^{-1}, BAI 5.14 μg ml^{-1}) was added to each well and incubate for further 8 h. The supernatant of the cell culture medium was collected after 300 g centrifugation for 10 min. The cytokine levels of IL-6, TNF-α and CXCL2 were detected by ELISA kits.

2.14. Lung targeting capability of the dead cells

J774A.1 dead cells were labelled with cy5.5-NHS to obtain fluorescence-tagged dead cells. Free cy5.5 and cy5.5-dead cell were intravenously injected into Balb/c mice with cy5.5 dose of 8 μg per mice. The mice were sacrificed at 0.5 h, 1 h and 1.5 h, respectively, and typical tissues of heart, liver, spleen, lung and kidney were dissected and imaged by IVIS imaging system. The fluorescence signal was analyzed by the software of Living Image.

Balb/c mice were randomly divided into following groups: DEX (5 mg kg^{-1}), BAI (BAI 1.56 mg kg^{-1}), DEX&BAI/Dead cell (DEX 5 mg kg^{-1}, BAI 1.56 mg kg^{-1}, 2×10^6 dead cells). After 1 h of the drug intravenous administration, the mice were sacrificed. The tissues of heart, liver, spleen, lung and kidney were taken out, washed with normal saline and dried with filter paper. After the tissue was homogenized and concentrated, the drug concentration in each tissue was detected by HPLC.

2.15. In vivo anti-inflammation efficacy in LPS-induced pneumonia model

Balb/c mice were anesthetized with isoflurane and 50 μl LPS (10 mg kg^{-1}) was instilled into the trachea by endotracheal intubation to set up the pneumonia model. The mice were randomly divided into following groups: saline, dead cell (2×10^6), DEX (5 mg kg^{-1}), DEX&BAI (DEX 5 mg kg^{-1}, BAI 1.56 mg kg^{-1}), DEX/Dead cell (DEX 5 mg kg^{-1}, 2×10^6 dead cells), DEX&BAI/Dead cell (DEX 5 mg kg^{-1}, BAI 1.56 mg kg^{-1}, 2×10^6 dead cells). 4 h later, the drugs were injected through the tail vein. 24 h post-instillation of LPS, 400 μl blood was collected *via* the orbital vein into the serum collection tubes and centrifuged for 10 min at 3000 rpm. The serum cytokine levels of IL-6, TNF-α, IL-1β and CXCL2 were determined by Elisa kits. After blood collection, the mice were sacrificed and bronchoalveolar lavage fluid was collected. In brief, 22G catheter was inserted into trachea and 1 ml cold PBS (containing 100 μM EDTA) was slowly injected into the lungs for lavage. The lavage fluid was recovered within 2 min and repeated 3 times. The supernatant was obtained by 3000 rpm centrifugation for 10 min to evaluate the protein level in the bronchoalveolar lavage fluid by BCA protein detection kit. The precipitated cells were re-suspended and first incubated with 200 μl red blood cell lysate for 2 min. Then 1 ml cold PBS was added to stop the lysis and centrifuged at 400 g for 7 min. The remaining cells were resuspended in PBS (1% FBS) and the percentages of macrophage ($F4/80^+CD11b^+$) and neutrophil ($Ly6G^+CD11b^+$) were analyzed by flow cytometry after antibody staining. The lung tissues were scissored out for following assays. The right lung lobe was paraffin-embedded and sliced for HE staining. The left lung lobe was weighed as the wet weight, and the dry weight was recorded after drying at 60 °C for 72 h. The wet/dry weight ratio of the lung tissue was calculated to evaluate the extent of pulmonary edema. To evaluate the survival of the mice of different groups, the procedures of modeling and treatments were same as stated above, and the mice survival was recorded daily.

2.16. Statistical analysis

The data were expressed as mean ± SD. The data were analyzed by Student's t-test between two groups and one-way ANOVA of three or more groups. The survival curve was analyzed by Mantel Cox test. All statistical analysis were conducted with GraphPad Prism and Compusyn software. The threshold of a statistically significant difference was defined as $P < 0.05$.

3. Results

3.1. Engineering of the immunosuppressive dead cell

The immunosuppressive dead cell was engineered by one-time quick shock of the live immune cells in liquid nitrogen. In specific, the murine mononuclear macrophage J774A.1 cells were first suspended in cell suspension medium and immersed in liquid nitrogen. Before use, the cells were thawed at 37 °C and washed with PBS. The preparation procedure was illustrated in Fig. 1. DMSO percentage in the suspension medium was crucial to the state of obtained dead cells. The cellular structure was severely damaged and more easily to be disintegrated after treating with liquid nitrogen if decreasing the percentage of DMSO. However, high DMSO percentage could not guarantee that all the cells lost proliferation capability. After evaluation, the formula of the cell suspension medium was set as 75%DMEM, 20%FBS and 5%DMSO in this work (Fig. S1). The cellular structure of the obtained J774A.1 dead cell was viewed by laser confocal microscope and SEM. J774A.1 dead cell maintained approximately intact cellular structure as the live cells after staining nucleus and cytoskeleton with the cellular size of 10–20 μm (Fig. 2A and B, Fig. S2). Next, the cell activity of the obtained dead cells was tested. As shown in Fig. 2C, all dead cells were labelled with PI (representing dead cells), but did not display the fluorescent signal of calcein AM (representing live cells). In addition, J774A.1 dead cells could not proliferate any more which was verified by CCK-8 assay (Fig. 2D) and exhibited necrosis-depended cell death (Fig. S3). We further tested the cytokine secretion function of J774A.1 dead cells after stimulation by LPS. As shown in Fig. 2E, the levels of IL-6, CXCL2 and TNF-α was sharply increased after stimulation for live J774A.1 cells, while there was little change for the dead cells. Meanwhile, the immune activation effect of the prepared dead cells was also analyzed. We added J774A.1 dead cells (1×10^5 per well) in the cell culturing plate containing live macrophages (1×10^5 per well). As shown in Fig. S4, the cytokine levels changed little between the dead cell group and saline group.

Furthermore, the biosafety of the dead cells was evaluated *in vivo*. 2×10^6 J774A.1 dead cells were intravenously injected into the healthy mice, and all the mice survived for at least 90 days (Fig. 2F). In addition, we injected 2×10^6 J774A.1 dead cells into the LPS-induced pneumonia mice. As shown in Fig. 2G, the injection of J774A.1 dead cells significantly elongated the survival of mice compared to untreated group, whereas the survival was significantly shortened if injecting live J774A.1 cells. We also quantitatively analyzed the serum cytokine levels of the LPS-induced pneumonia mice after injection of live and dead J774A.1 cells. Lower cytokine levels of IL-6, TNF-α, IL-1β and CXCL2 were detected for dead cell group, while significantly higher for live cell group (Fig. 2H). Above date certified the biosafety of J774A.1 dead cells to be used as biofunctional material *in vivo*.

3.2. Preparation of drug-loading dead cells (DEX&Bai/Dead cell)

DEX is a synthetic glucocorticoid that can inhibit the inflammatory cascade. Due to its strong anti-inflammatory effects, DEX is widely used in the treatment of a variety of acute and chronic inflammatory diseases, and low-dose DEX is also recommended for the treatment of COVID-19 in clinic [23,24]. However, large dose and repeated administration of dexamethasone will lead to drug resistance and serious local and systemic side effects, such as osteoporosis and femoral head necrosis [25]. BAI is one of the main flavonoid extracts extracted from Scutellaria baicalensis, which is widely used in the combination therapy of COVID-19 in clinic in China [24,26]. Thus, we choose the combination of DEX and BAI to achieve the synergistic anti-inflammation effects.

DEX and BAI were co-loaded in J774A.1 dead cells to decrease the drug dose and side effects of the glucocorticoid drug dexamethasone. We

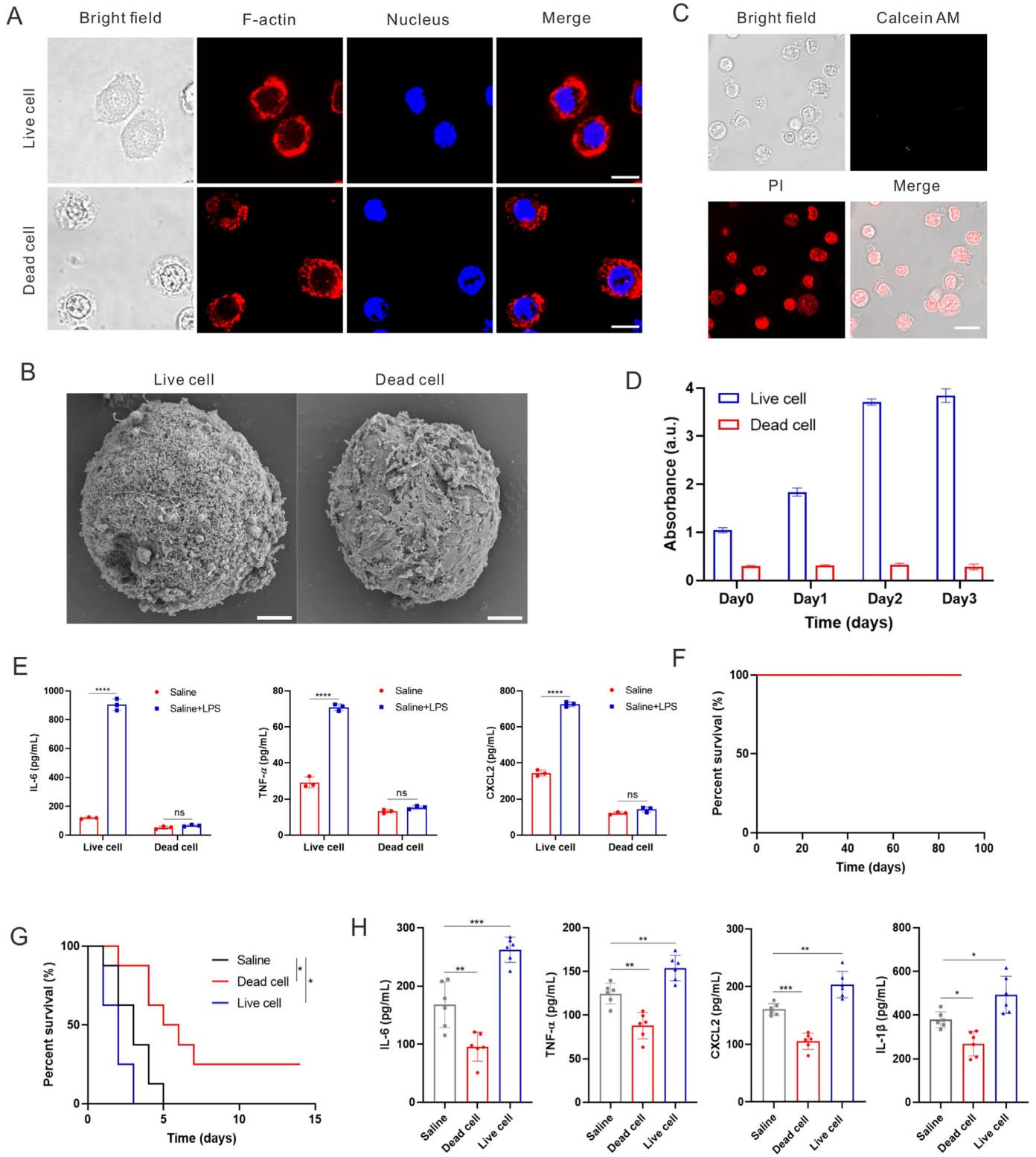

Fig. 2. Preparation and characterization of J774A.1 dead cells. (A) Confocal fluorescence images of the live and dead J774A.1 cells. The nucleus was stained with Hoechst 33,342 (blue) and the cytoplasmic F-actin was stained with rhodamine Phalloidin (red). Scale bar, 10 μm. (B) Scanning electron microscope images of the live and dead J774A.1 cells. Scale bar, 2 μm. (C) The cell state of the prepared J774A.1 dead cells with Live/Dead staining assay. Calcein AM: live cells; PI: dead cells. Scale bar, 10 μm. (D) Cell proliferation capability of the cells analyzed by CCK-8 assay ($n = 6$). (E) Cytokines secretion of indicated groups after LPS activation ($n = 3$) The LPS concentration was 50 ng ml^{-1} and dead cell of 1×10^5 cells per well. (F) Survival of mice after challenge with 2×10^6 J774A.1 dead cells ($n = 6$). (G) Survival of pneumonia mice after injection of 2×10^6 live or dead J774A.1 cells ($n = 8$). (H) Cytokine levels in pneumonia mice after injection of 2×10^6 live or dead J774A.1 cells ($n = 6$). Statistical significance was calculated *via* Student's *t*-test (E), Mantel Cox test (G) and ordinary one-way ANOVA (H). All data are expressed as mean ± SD, $^*P < 0.05$, $^{**}P < 0.01$, $^{***}P < 0.001$. (For interpretation of the references to color in this figure legend, the reader is referred to the Web version of this article.)

first investigate the combination ratio of the two drugs to achieve the synergetic anti-inflammatory effects. As shown in Fig. 3A, the half inhibitory concentrations (IC_{50}) of DEX and BAI on IL-6 secretion of J774A.1 cells were 5.14 μM and 19.67 μM, respectively. The combination of DEX and BAI could amplify the anti-inflammatory effect with a wide combination ratio from 19:1 to 1:19 (95% $IC_{50,DEX}$ +5% $IC_{50,BAI}$ to 5% $IC_{50,DEX}$ +95% $IC_{50,BAI}$), and the combination ratio of 14:1 (93.33% $IC_{50,DEX}$ +6.67% $IC_{50,BAI}$) achieve highest inhibition efficacy, which was significantly better than that of DEX or BAI alone (Fig. 3B, Table S1).

Then drugs were loaded in the dead cells *via* electrostatic interactions between dead cells and drug-loaded cationic liposomes. As shown in Fig. 3C, obvious fluorescence signal could be detected in the dead cells when utilizing coumarin-6 (Cou-6) as the model drug. The loading capacities of DEX and BAI in DEX&BAI/Dead cell was 65.65 ± 1.62 μg and 20.54 ± 1.04 μg per 1×10^6 J774A.1 dead cell, respectively, realizing the combination mol ratio of 14:1 (Fig. 3D).

According to literature, the shearing stress of blood flow in pulmonary capillaries is around 6 Pa [27,28], thus we evaluated the drug release behavior of DEX&BAI/Dead cell under different shearing forces (0 Pa, 2 Pa, 6 Pa) with a peristaltic pump to mimic the blood flow *in vitro* after adjusting the circulation speed. During circulation, the drug-loaded liposomes absorbed on the dead cell could fall off, and the drug shedding ratio was only 17.2% within 1 h under static conditions (0 Pa), while the ratio increased to 37.5% under low shearing stress of 2 Pa (blood stream) and 56.4% under 6 Pa (pulmonary capillaries) (Fig. 3E). Meanwhile, the drugs were also released from DEX&BAI/Lip in a sustained manner (Fig. S5).

3.3. Lung targeting capability of dead cells

Particles, of which the particle size are over 7 μm [29–32], could passively target to the lung due to the interception by pulmonary capillaries. The particle size of dead cells was between 10 μm and 20 μm (Fig. 2A and B), which could be leveraged as the lung targeting vehicle. After labelling with the fluorescence dye of cy5.5, obvious fluorescence signal could be observed in the lung tissue and significantly stronger than that of free cy5.5 within 1 h post-injection (Fig. 4A and B), which guaranteed the drug accumulation in the lung after intravenous injection of drug-loaded dead cells regarding the fast release of drugs under the sheer stress of lung capillary. As shown in Fig. 4C and D, the concentrations of DEX and BAI in the lungs were increased by 1.9 times and 1.7 times compared to the free drug group, respectively.

3.4. Expression of J774A.1 dead cell surface proteins

Immune cells express various receptors to bind cytokines and exogenous substances to induce immune responses. For the dead cell, these receptors were still maintained, various inflammation-related receptors of CD14 (LPS receptor), TLR4 (LPS receptor), gp130 (IL-6 receptor), CD121a (IL-1β receptor), CXCR2 (CXCL2 receptor) and CD120a (TNF-α receptor) were expressed on J774A.1 dead cells, which was similar as that of live J774A.1 cells (Fig. 5A and B) as analyzed by laser confocal microscopy and flow cytometry. The cytokine receptors on the surface of these dead cells enabling the dead cells to "capture" cytokines and reduce the extent of inflammatory response. As shown in Fig. 5C, clear fluorescence signal of FAM-labelled IL-6 could be observed after incubation with the dead cells. Further, we also detected the concentration change of free IL-6 that could be detected by Elisa kit after incubating with dead cells. As shown in Fig. 5D, IL-6 concentration was significantly lowered after the incubation. Above data certified the cytokine absorption capability of the dead cells.

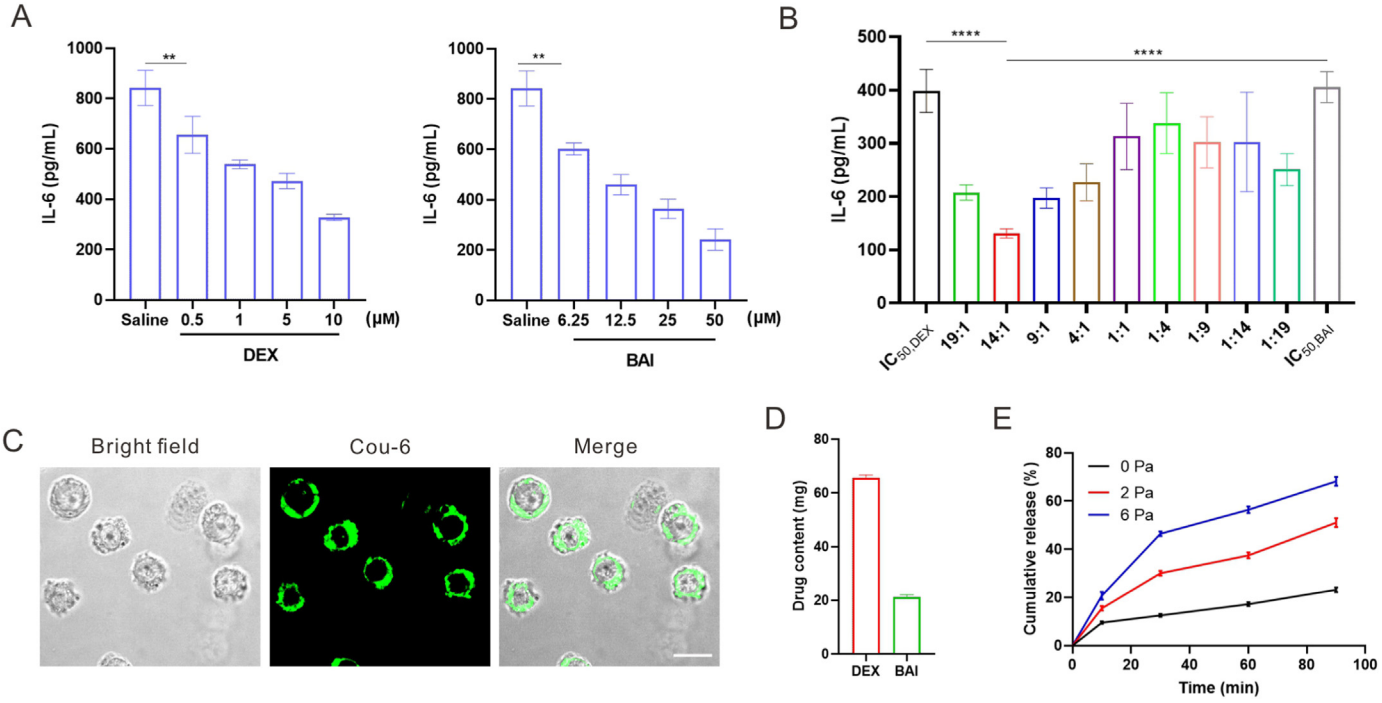

Fig. 3. *In vitro* drug loading and release. (A) IL-6 secretion of J774A.1 cells activated by LPS after treatment with DEX or BAI ($n = 3$). (B) IL-6 secretion of J774A.1 cells after treatment with indicated combined proportions of DEX and BAI ($n = 3$). 19:1 indicated 95% $IC_{50,DEX}$ +5% $IC_{50,BAI}$; 14:1 indicated 93.33% $IC_{50,DEX}$ +6.67% $IC_{50,BAI}$; 9:1 indicated 90% $IC_{50,DEX}$ +10% $IC_{50,BAI}$; 4:1 indicated 80% $IC_{50,DEX}$ +20% $IC_{50,BAI}$; 1:1 indicated 50% $IC_{50,DEX}$ +50% $IC_{50,BAI}$; 1:4 indicated 20% $IC_{50,DEX}$ +80% $IC_{50,BAI}$; 1:9 indicated 10% $IC_{50,DEX}$ +90% $IC_{50,BAI}$; 1:14 indicated 6.67% $IC_{50,DEX}$ +93.33% $IC_{50,BAI}$; 1:19 indicated 5% $IC_{50,DEX}$ +95% $IC_{50,BAI}$. (C) Typical confocal images of drug-loaded dead cells (green fluorescence: coumarin 6). Scale bar, 10 μm. (D) The loading capacity of DEX and BAI per 1×10^6 J774A.1 dead cell ($n = 3$). (E) Drug release from J774A.1 dead cells under indicated shearing forces ($n = 3$). Statistical significance was calculated *via* Student's *t*-test. All data are expressed as mean ± SD, $^*P < 0.05$, $^{**}P < 0.01$, $^{***}P < 0.001$. (For interpretation of the references to color in this figure legend, the reader is referred to the Web version of this article.)

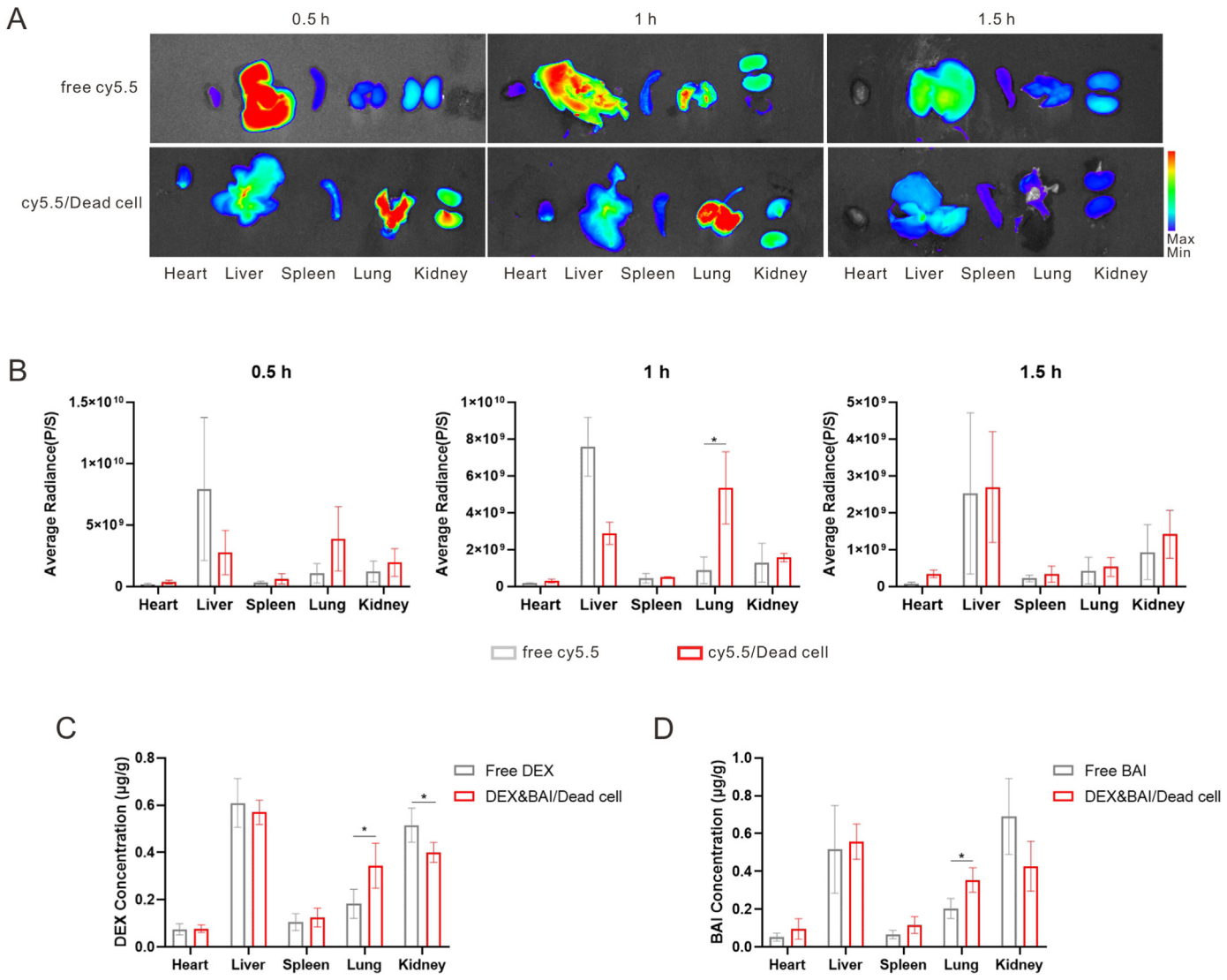

Fig. 4. Lung targeting capability of dead cells. (A) *In vivo* distribution of free cy5.5 and cy5.5-labelled dead cells. (B) Fluorescence radiance of major organs at indicated timepoints ($n = 3$). DEX (C) and BAI (D) tissue concentrations in mice after 1 h of *i. v.* administration of indicated formulation ($n = 4$). Statistical significance was calculated *via* Student's *t*-test. All data are expressed as mean ± SD, $^{*}P < 0.05$, $^{**}P < 0.01$.

3.5. Immunosuppression of dead cell and DEX&Bai/Dead cell in vitro

The immunosuppression efficacy of dead cells and drug-loaded dead cells were evaluated. First, J774A.1 dead cell could inhibit the activation and maturation of dendritic cells. After LPS stimulation, the biomarkers of CD80 and CD86 were elevated with 13.2% $CD80^{+}CD86^{+}$ DCs, while the number was only 6.6% if the existence of the dead cells (Fig. 6C and Fig. S6). The reason may attribute to the retention of LPS receptors on J774A.1 dead cells (Fig. 5B), enabling the absorption of the exogenous stimuli of LPS to some extent and inhibit its further contact with live immune cells.

Further, we measured the secretion of various cytokines of J774A.1 cells after LPS activation. As shown in Fig. 6B, the secreted cytokines of IL-6, CXCL2 and TNF-α by J774A.1 cells after LPS activation were significantly lowered if the culture medium containing J774A.1 dead cell and DEX&BAI/Dead cell, and this effect became more obvious after the incubation time longer than 4 h (Fig. 6C).

3.6. In vivo anti-inflammation efficacy in LPS-induced pneumonia model

The mice were intratracheally instilled LPS to build up the pneumonia model, and treated with different formulations of saline, dead cell, DEX, DEX&BAI and DEX&BAI/Dead cell (Fig. 7A). Compared with other groups, the degree of lung injury in DEX&BAI/Dead cell group was the most modest, with thinner alveolar walls and less inflammatory cell infiltration (Fig. 7B). The protein concentration in bronchoalveolar lavage fluid (BALF) could reflect the vascular permeability, and this value of DEX&BAI/Dead cell group was significantly lower than that of all other groups. Consistently, the wet/dry weight ratio which indicated the state of pulmonary edema also decreased most in mice treated with DEX&BAI/Dead cell (Fig. 7C and D). The immune cells in BALF were also evaluated by flow cytometry, the cell percentage of both neutrophils ($Ly6G^{+}CD11b^{+}$) and monocyte-derived macrophages ($F4/80^{+}CD11b^{+}$) were diminished after DEX&BAI/Dead cell treatment (Fig. 7E and F, Fig. S7). The serum cytokine levels are direct indicators to evaluate the anti-inflammation efficacy, and the cytokine levels of IL-6, TNF-α, CXCL2 and IL-1β were significantly decreased in DEX&BAI/Dead cell group (Fig. 7G). Moreover, DEX&BAI/Dead cell treatment elongated the survival of pneumonia mice. As shown in Fig. 7H, after LPS stimulation all the mice died at day 4 for saline group, while 83.3% mice still survived at day 14 post-stimulation of LPS for DEX&BAI/Dead cell group. Above data certified the anti-inflammation and cytokine storm attenuation efficacy

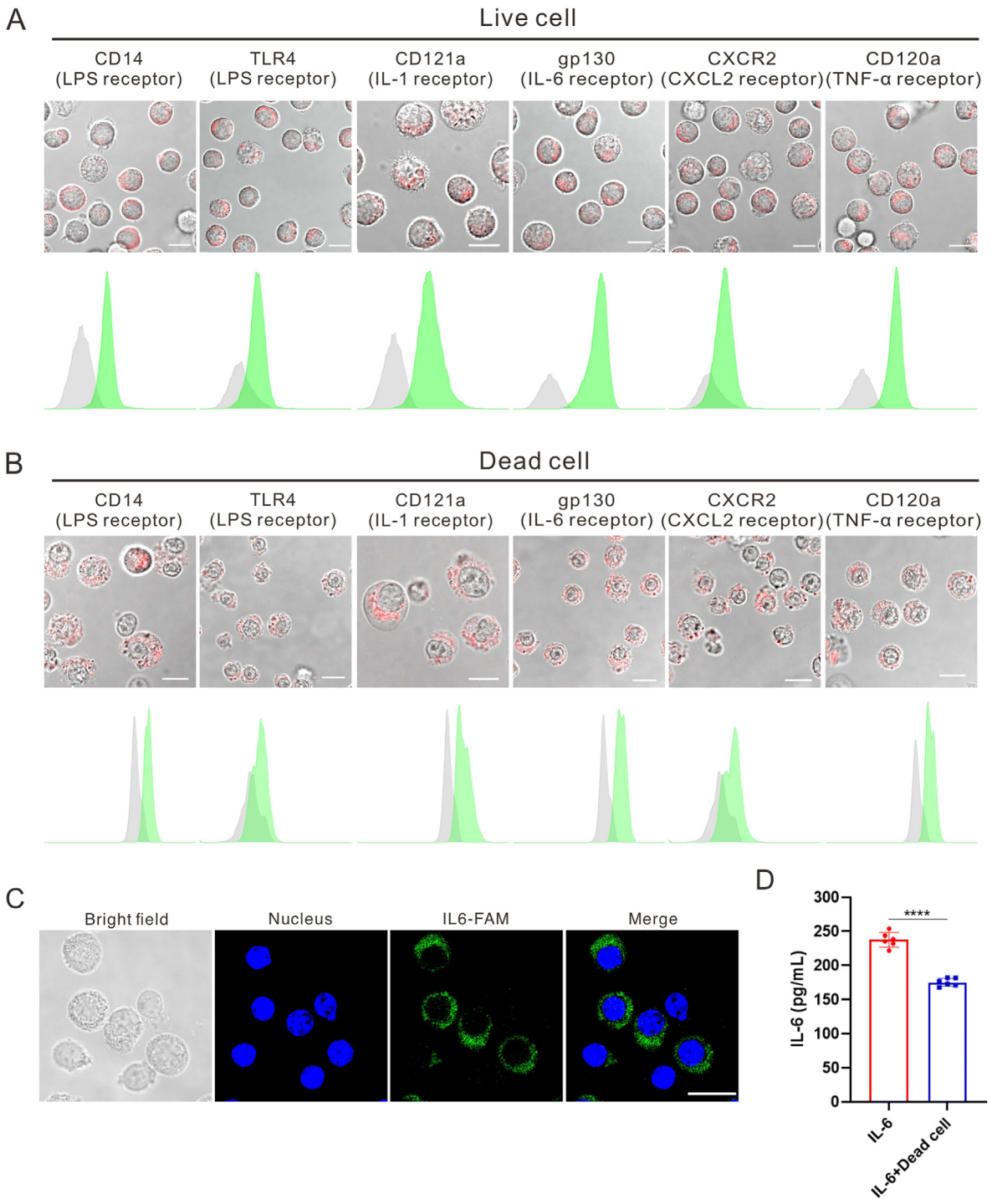

Fig. 5. Expression of J774A.1 dead cell surface proteins. Receptor expression of J774A.1 live cells (A) and dead cells (B) analyzed by confocal microscopy (top) and flow cytometry (bottom). Scale bars, 10 μm. (C) Laser confocal images of dead cells after incubating with FAM-labelled IL-6. Scale bar, 10 μm. (D) Changes of IL-6 concentration detected by Elisa kit after incubation with J774A.1 dead cells. ($n = 6$). The IL-6 concentration was 250 pg ml^{-1} and dead cell of 2×10^6 cells. Statistical significance was calculated *via* Student's *t*-test. All data are expressed as mean ± SD, $^{**}P < 0.01$, $^{***}P < 0.001$.

of the drug-loaded immune dead cells.

4. Discussion

Cell-derived vehicles are intriguing more interests in developing drug delivery systems due to their unique biological functions [33–48]. Herein, we focused on the function of the dead cells, that were engineered by the one-time quick shock of live cells with liquid nitrogen. The obtained J774A.1 (mononuclear macrophage cell line) dead cell was proved to be immunosuppressive, attributing to the retaining of typical cell membrane proteins of CXCR2 [49], CD120a [50], gp130 [51] and CD121a [52] on cell surface, which enabled the dead cells to "capture" various cytokines of IL-6, TNF- α, CXCL2 and IL-1β *in vivo* and reduce the severity of cytokine storm.

Besides function as the mixed antibodies of cytokines, the dead cell could also serve as lung-targeting carriers due to its cellular size (10–20 μm) that can be trapped by pulmonary capillaries to achieve passive targeting to the lungs. However, the key point is how to load the drugs.

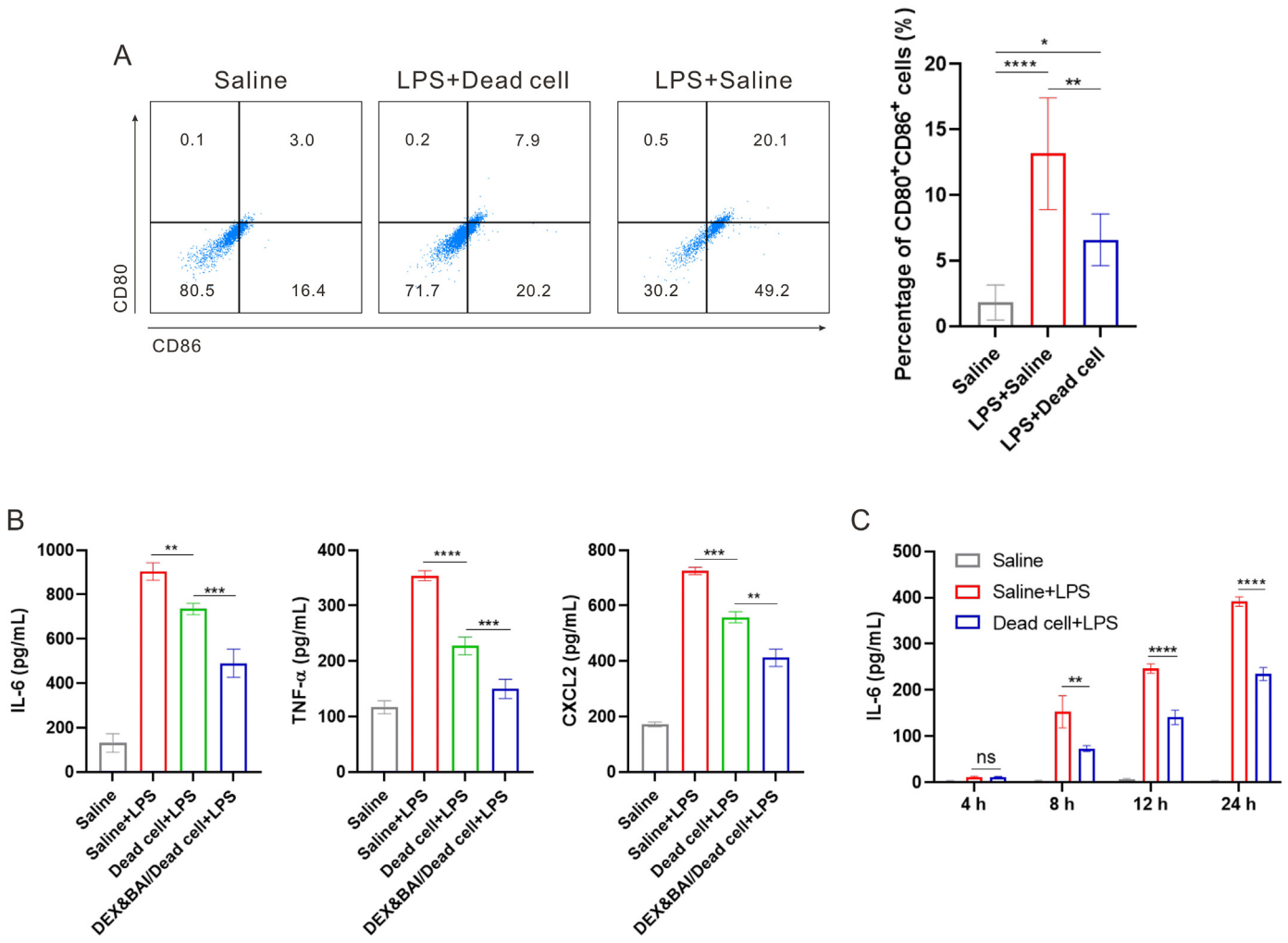

Fig. 6. *In vitro* immunosuppression of J774A.1 dead cell and DEX&BAI/Dead cell. (A) The maturation of dendritic cells 24 h post-LPS activation of $CD11c^+$ DC2.4 cells of indicated groups ($n = 6$). The LPS concentration was 50 ng ml^{-1} and dead cell of 1×10^6 cells per well. (B) Cytokine secretion of macrophages after treatment with indicated groups ($n = 3$). The LPS concentration was 50 ng ml^{-1} and dead cell of 1×10^5 cells per well, and DEX 16.41 μg ml^{-1}, BAI 5.14 μg ml^{-1}. (C) IL-6 secretion of J774A.1 cells activated by LPS after treatment with dead cells ($n = 3$). The LPS concentration was 50 ng ml^{-1} and dead cell of 1×10^5 cells per well. Statistical significance was calculated *via* ordinary one-way ANOVA (A and B) and Student's *t*-test (C). All data are expressed as mean ± SD, $^{**}P < 0.01$, $^{***}P < 0.001$.

Direct chemical modification of the drugs or drug-loaded particles to the dead cell will influence the activity of membrane proteins to some extent and inhibit the capability of "cytokine antibodies" of the dead cells. Thus, we load the drugs by physical forces, that drug-loaded cationic liposomes were adsorbed on the surface of J774A.1 dead cells by electrostatic interaction. The loading capacity of dexamethasone on J774A.1 dead cells reached to 65 μg per 1×10^6 dead cell, which could satisfy the clinical drug dosing requirement (5 mg kg^{-1}). After intravenous injection, the adsorbed drugs could fall off from the dead cells due to the high vascular shearing force in lung capillaries, then the dead cells further behave as the mixed antibodies as stated before. This formulation design guaranteed the effectivity of the drug-loaded dead cells in the treatment of pneumonia.

In this work, the anti-inflammatory efficacy was attributed to the synergistic anti-inflammatory effects of anti-inflammatory drugs and the cytokine adsorption capability of the drug carrier. The dead cells serve as lung targeting vehicle to deliver drugs to the lung and exert anti-inflammatory efficacy after drug releasing, which exhibited advantages to other red blood cell or membrane-coated nanoparticles to some extent. In specific, the immunosuppressive dead cell exhibited better anti-inflammation capability than erythrocyte-based vehicles, and easy production process than other membrane-based systems.

This freeze-shock cell engineering technology is feasible to good manufacturing practice (GMP) and the drug loading procedures are also easy to operate, which enabled the feasibility of the quality control of the drug-loaded dead cell in practical use. In addition, besides the mononuclear macrophage J774A.1, other immune cells that act in the progressing of cytokine storm in pneumonia might also utilize this liquid-nitrogen shocking technique to engineer the immunosuppressive dead cell, and the potential of the universality could be evaluated in the future.

5. Conclusions

An immunosuppressive dead cell was engineered as drug lung-targeting carrier and cytokine absorption material, to exhibit synergetic anti-inflammation efficacy in the treatment of pneumonia.

Credit author statement

TY Ci: conceptualization, methodology, supervision, analyzing and interpreting the data, funding acquisition, manuscript writing-review and editing. **YX Xiong:** methodology, experimental work, data curation, manuscript original draft. **JN Zhang:** data curation, methodology, experimental work. **J Zang:** methodology, experimental work. **NP Feng:** supervision, funding acquisition, manuscript writing-review and editing.

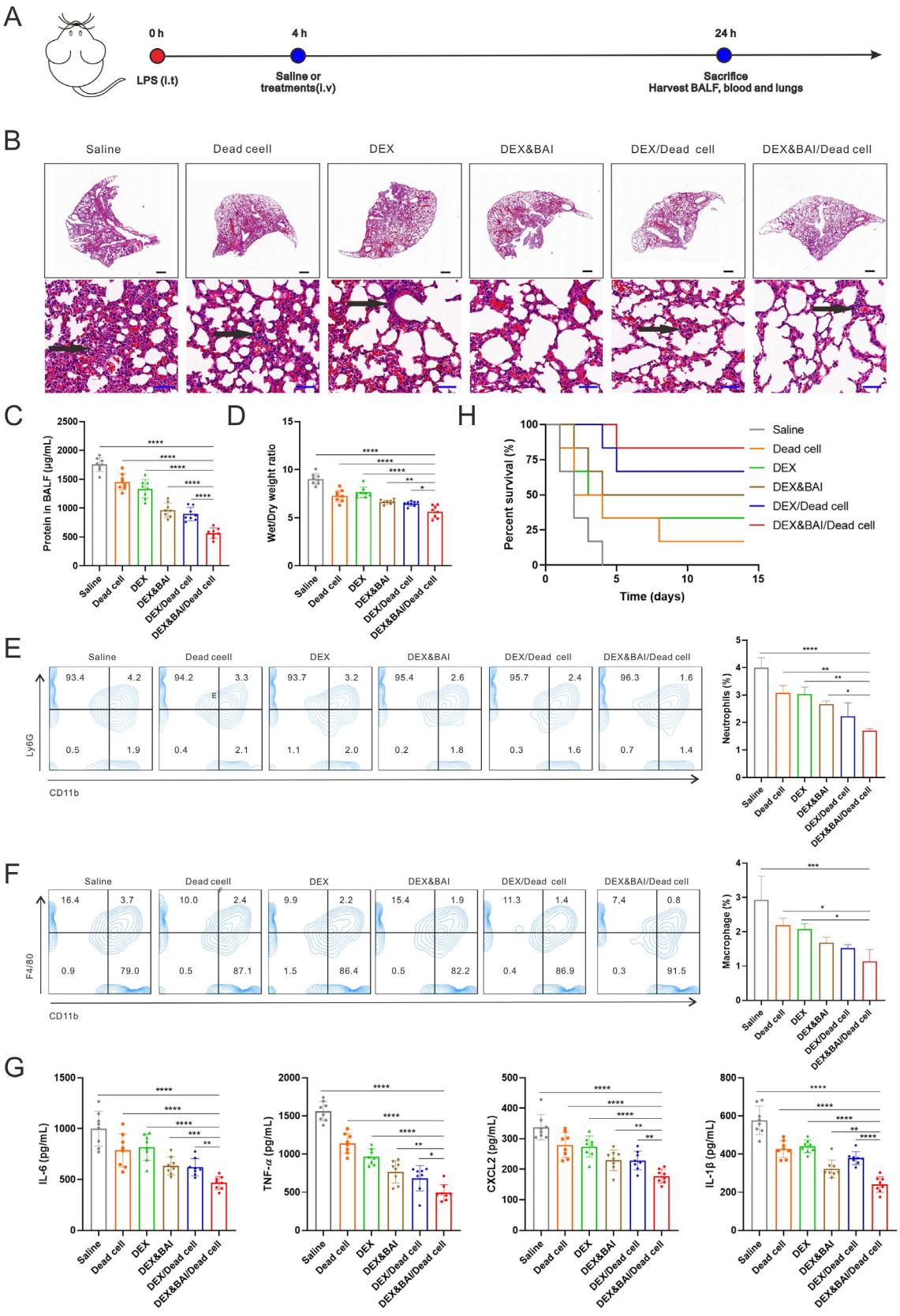

Fig. 7. *In vivo* anti-inflammation efficacy. (A) The scheme of LPS-induced pneumonia model set-up and treatments. (B) Representative H&E staining of lung tissues (Black arrow: inflammatory cell infiltration). Scale bars, 500 μm (upper line) and 50 μm (lower line). (C) Total protein level in the BAL fluid ($n = 8$). (D) Wet-dry weight ratio of lung tissue ($n = 8$). (E) Flow cytometry analysis of neutrophils ($CD11b^+$ $Ly6G^+$) in BAL fluid ($n = 3$). (F) Flow cytometry analysis of macrophages ($CD11b^+$ $F4/80^+$) in BAL fluid ($n = 3$). (G) Serum cytokine levels ($n = 8$). (H) Survival of the mice of different treatment groups ($n = 6$). Statistical significance was calculated *via* ordinary one-way ANOVA. All data are expressed as mean ± SD, $^*P < 0.05$, $^{**}P < 0.01$, $^{***}P < 0.001$.

Declaration of competing interest

The authors declare that they have no known competing financial interests or personal relationships that could have appeared to influence the work reported in this paper.

Data availability

Data will be made available on request.

Acknowledgments

This work was supported by National Natural Science Foundation of China (No. 82173984), Shanghai Rising-Star Program (No. 21QA1408800), Program for Shanghai High-Level Local University Innovation Team (SZY20220315).

Appendix B. Supplementary data

Supplementary data to this article can be found online at https://doi.org/10.1016/j.mtbio.2023.100684.

References

[1] A. Torres, C. Cilloniz, M.S. Niederman, et al., Pneumonia, Nat. Rev. Dis. Prim. 7 (2021) 25, https://doi.org/10.1038/s41572-021-00259-0.
[2] L.J. Quinton, A.J. Walkey, J.P. Mizgerd, Integrative physiology of pneumonia, Physiol. Rev. 98 (2018) 1417–1464, https://doi.org/10.1152/physrev.00032.2017.
[3] R. Karki, T.D. Kanneganti, The 'cytokine storm': molecular mechanisms and therapeutic prospects, Trends Immunol. 42 (2021) 681–705, https://doi.org/10.1016/j.it.2021.06.001.
[4] X.Q. Liu, S. Xue, J.B. Xu, et al., Clinical characteristics and related risk factors of disease severity in 101 covid-19 patients hospitalized in wuhan, China, Acta Pharmacol. Sin. 43 (2022) 64–75, https://doi.org/10.1038/s41401-021-00627-2.
[5] D.C. Fajgenbaum, C.H. June, Cytokine storm, N. Engl. J. Med. 383 (2020) 2255–2273, https://doi.org/10.1056/NEJMra2026131.
[6] N. Mangalmurti, C.A. Hunter, Cytokine storms: understanding covid-19, Immunity 53 (2020) 19–25, https://doi.org/10.1016/j.immuni.2020.06.017.
[7] R. Channappanavar, S. Perlman, Pathogenic human coronavirus infections: causes and consequences of cytokine storm and immunopathology, Semin. Immunopathol. 39 (2017) 529–539, https://doi.org/10.1007/s00281-017-0629-x.
[8] K.K. To, I.F. Hung, I.W. Li, et al., Delayed clearance of viral load and marked cytokine activation in severe cases of pandemic h1n1 2009 influenza virus infection, Clin. Infect. Dis. 50 (2010) 850–859, https://doi.org/10.1086/650581.
[9] C. Solinas, L. Perra, M. Aiello, et al., A critical evaluation of glucocorticoids in the management of severe covid-19, Cytokine Growth Factor Rev. 54 (2020) 8–23, https://doi.org/10.1016/j.cytogfr.2020.06.012.
[10] Y. Chen, K. Li, H. Pu, et al., Corticosteroids for pneumonia, Cochrane Db Syst Rev 16 (2011), Cd007720, https://doi.org/10.1002/14651858.CD007720.pub2.
[11] J.B. Parr, Time to reassess tocilizumab's role in covid-19 pneumonia, JAMA Intern. Med. 181 (2021) 12–15, https://doi.org/10.1001/jamainternmed.2020.6557.
[12] L. Yang, X. Xie, Z. Tu, et al., The signal pathways and treatment of cytokine storm in covid-19, Signal Transduct Tar 6 (2021) 255, https://doi.org/10.1038/s41392-021-00679-0.
[13] J.Y. Park, S. Kwon, S.H. Kim, et al., Triamcinolone-gold nanoparticles repolarize synoviocytes and macrophages in an inflamed synovium, Acs Appl Mater Inter 12 (2020) 38936–38949, https://doi.org/10.1021/acsami.0c09842.
[14] R. Zhao, H. Wang, X. Wang, et al., Steroid therapy and the risk of osteonecrosis in sars patients: a dose-response meta-analysis, Osteoporosis Int. 28 (2017) 1027–1034, https://doi.org/10.1007/s00198-016-3824-z.
[15] J.F. Griffith, G.E. Antonio, S.M. Kumta, et al., Osteonecrosis of hip and knee in patients with severe acute respiratory syndrome treated with steroids, Radiology 235 (2005) 168–175, https://doi.org/10.1148/radiol.2351040100.
[16] H. Wang, H. Liu, J. Li, et al., Cytokine nanosponges suppressing overactive macrophages and dampening systematic cytokine storm for the treatment of hemophagocytic lymphohistiocytosis, Bioact. Mater. 21 (2023) 531–546, https://doi.org/10.1016/j.bioactmat.2022.09.012.
[17] A.S. Chau, A.G. Weber, N.I. Maria, et al., The longitudinal immune response to coronavirus disease 2019: chasing the cytokine storm, Arthritis Rheumatol. 73 (2021) 23–35, https://doi.org/10.1002/art.41526.
[18] L.J. Quinton, J.P. Mizgerd, Dynamics of lung defense in pneumonia: resistance, resilience, and remodeling, Annu. Rev. Physiol. 77 (2015) 407–430, https://doi.org/10.1146/annurev-physiol-021014-071937.
[19] M. Zoulikha, Q. Xiao, G.F. Boafo, et al., Pulmonary delivery of sirna against acute lung injury/acute respiratory distress syndrome, Acta Pharm. Sin. B 12 (2022) 600–620, https://doi.org/10.1016/j.apsb.2021.08.009.
[20] M. Dukhinova, E. Kokinos, P. Kuchur, et al., Macrophage-derived cytokines in pneumonia: linking cellular immunology and genetics, Cytokine Growth Factor Rev. 59 (2021) 46–61, https://doi.org/10.1016/j.cytogfr.2020.11.003.
[21] J. Liu, M. Wan, C.J. Lyon, et al., Nanomedicine therapies modulating macrophage dysfunction: a potential strategy to attenuate cytokine storms in severe infections, Theranostics 10 (2020) 9591–9600, https://doi.org/10.7150/thno.47982.
[22] T. Ci, H. Li, G. Chen, et al., Cryo-shocked cancer cells for targeted drug delivery and vaccination, Sci. Adv. 6 (2020), https://doi.org/10.1126/sciadv.abc3013 eabc3013.
[23] T. Asselah, D. Durantel, E. Pasmant, et al., Covid-19: discovery, diagnostics and drug development, J. Hepatol. 74 (2021) 168–184, https://doi.org/10.1016/j.jhep.2020.09.031.
[24] Y.H. Jin, Q.Y. Zhan, Z.Y. Peng, et al., Chemoprophylaxis, diagnosis, treatments, and discharge management of covid-19: an evidence-based clinical practice guideline (updated version), Mil Med Res 7 (2020) 41, https://doi.org/10.1186/s40779-020-00270-8.
[25] J.F. Griffith, G.E. Antonio, S.M. Kumta, et al., Osteonecrosis of hip and knee in patients with severe acute respiratory syndrome treated with steroids, Radiology 235 (2005) 168–175, https://doi.org/10.1148/radiol.2351040100.
[26] Y.H. Jin, L. Cai, Z.S. Cheng, et al., A rapid advice guideline for the diagnosis and treatment of 2019 novel coronavirus (2019-ncov) infected pneumonia (standard version), Mil Med Res 7 (2020) 4, https://doi.org/10.1186/s40779-020-0233-6.
[27] A.C. Anselmo, V. Gupta, B.J. Zern, et al., Delivering nanoparticles to lungs while avoiding liver and spleen through adsorption on red blood cells, ACS Nano 7 (2013) 11129–11137, https://doi.org/10.1021/nn404853z.
[28] Z. Zhao, A. Ukidve, V. Krishnan, et al., Systemic tumour suppression via the preferential accumulation of erythrocyte-anchored chemokine-encapsulating nanoparticles in lung metastases, Nat Biomed Eng 5 (2021) 441–454, https://doi.org/10.1038/s41551-020-00644-2.
[29] X. Lin, J. He, W. Li, et al., Lung-targeting lysostaphin microspheres for methicillin-resistant staphylococcus aureus pneumonia treatment and prevention, ACS Nano 15 (2021) 16625–16641, https://doi.org/10.1021/acsnano.1c06460.
[30] M. Agnoletti, C. Rodríguez-Rodríguez, S.N. Kłodzińska, et al., Monosized polymeric microspheres designed for passive lung targeting: biodistribution and pharmacokinetics after intravenous administration, ACS Nano 14 (2020) 6693–6706, https://doi.org/10.1021/acsnano.9b09773.
[31] C.L. Fang, C.J. Wen, I.A. Aljuffali, et al., Passive targeting of phosphatiosomes increases rolipram delivery to the lungs for treatment of acute lung injury: an animal study, J. Contr. Release 213 (2015) 69–78, https://doi.org/10.1016/j.jconrel.2015.06.038.
[32] H.L. Kutscher, P. Chao, M. Deshmukh, et al., Threshold size for optimal passive pulmonary targeting and retention of rigid microparticles in rats, J. Contr. Release 143 (2010) 31–37, https://doi.org/10.1016/j.jconrel.2009.12.019.
[33] Z. Zhao, L. Fang, P. Xiao, et al., Walking dead tumor cells for targeted drug delivery against lung metastasis of triple-negative breast cancer, Adv. Mater. 34 (2022), e2205462, https://doi.org/10.1002/adma.202205462.
[34] X. Liu, J. Xu, T. Yao, et al., Cryo-shocked cancer cells as an oncolytic adenovirus reservoir for glioblastoma immunotherapy, Acs Appl Mater Inter 15 (2023) 67–76, https://doi.org/10.1021/acsami.2c16806.
[35] J. Li, Y. Ding, Q. Cheng, et al., Supramolecular erythrocytes-hitchhiking drug delivery system for specific therapy of acute pneumonia, J. Contr. Release 350 (2022) 777–786, https://doi.org/10.1016/j.jconrel.2022.08.029.
[36] Y. Ding, B. Lv, J. Zheng, et al., Rbc-hitchhiking chitosan nanoparticles loading methylprednisolone for lung-targeting delivery, J. Contr. Release 341 (2022) 702–715, https://doi.org/10.1016/j.jconrel.2021.12.018.
[37] R.H. Fang, W. Gao, L. Zhang, Targeting drugs to tumours using cell membrane-coated nanoparticles, Nat. Rev. Clin. Oncol. 20 (2023) 33–48, https://doi.org/10.1038/s41571-022-00699-x.
[38] X. Wei, D. Ran, A. Campeau, et al., Multiantigenic nanotoxoids for antivirulence vaccination against antibiotic-resistant gram-negative bacteria, Nano Lett. 19 (2019) 4760–4769, https://doi.org/10.1021/acs.nanolett.9b01844.
[39] F. Zhang, J. Zhuang, Z. Li, et al., Nanoparticle-modified microrobots for in vivo antibiotic delivery to treat acute bacterial pneumonia, Nat. Mater. 21 (2022) 1324–1332, https://doi.org/10.1038/s41563-022-01360-9.
[40] J. Zhou, C.J. Ventura, Y. Yu, et al., Biomimetic neutrophil nanotoxoids elicit potent immunity against acinetobacter baumannii in multiple models of infection, Nano Lett. 22 (2022) 7057–7065, https://doi.org/10.1021/acs.nanolett.2c01948.
[41] Y. Xiao, C. Ren, G. Chen, et al., Neutrophil membrane-mimicking nanodecoys with intrinsic anti-inflammatory properties alleviate sepsis-induced acute liver injury and lethality in a mouse endotoxemia model, Mater Today Bio 14 (2022), 100244, https://doi.org/10.1016/j.mtbio.2022.100244.
[42] F. Wang, Q. Yu, J. Li, et al., Biomimetic macrophage membrane-coated gold-quantum dots with tumor microenvironment stimuli-responsive capability for tumor theranostic, Mater Today Bio 16 (2022), 100359, https://doi.org/10.1016/j.mtbio.2022.100359.
[43] L. Zhu, Y. Zhong, S. Wu, et al., Cell membrane camouflaged biomimetic nanoparticles: focusing on tumor theranostics, Mater Today Bio 14 (2022), 100228, https://doi.org/10.1016/j.mtbio.2022.100228.
[44] J. Dai, Z. Chen, S. Wang, et al., Erythrocyte membrane-camouflaged nanoparticles as effective and biocompatible platform: either autologous or allogeneic erythrocyte-derived, Mater Today Bio 15 (2022), 100279, https://doi.org/10.1016/j.mtbio.2022.100279.
[45] W. Zhang, X. Huang, Stem cell membrane-camouflaged targeted delivery system in tumor, Mater Today Bio 16 (2022), 100377, https://doi.org/10.1016/j.mtbio.2022.100377.
[46] S. Shen, H. Dai, Z. Fei, et al., Immunosuppressive nanoparticles for management of immune-related adverse events in liver, ACS Nano 15 (2021) 9111–9125, https://doi.org/10.1021/acsnano.1c02391.

[47] L. Zhang, W. Zhang, H. Peng, et al., Bioactive cytomembrane@poly(citrate-peptide)-mirna365 nanoplatform with immune escape and homologous targeting for colon cancer therapy, Mater Today Bio 15 (2022), 100294, https://doi.org/10.1016/j.mtbio.2022.100294.
[48] H. Dai, Q. Fan, C. Wang, Recent applications of immunomodulatory biomaterials for disease immunotherapy, Explorations 2 (2022), 20210157, https://doi.org/10.1002/EXP.20210157.
[49] K. Liu, L. Wu, S. Yuan, et al., Structural basis of cxc chemokine receptor 2 activation and signalling, Nature 585 (2020) 135–140, https://doi.org/10.1038/s41586-020-2492-5.
[50] N. Zhang, Z. Wang, Y. Zhao, Selective inhibition of tumor necrosis factor receptor-1 (tnfr1) for the treatment of autoimmune diseases, Cytokine Growth Factor Rev. 55 (2020) 80–85, https://doi.org/10.1016/j.cytogfr.2020.03.002.
[51] M. Murakami, D. Kamimura, T. Hirano, Pleiotropy and specificity: insights from the interleukin 6 family of cytokines, Immunity 50 (2019) 812–831, https://doi.org/10.1016/j.immuni.2019.03.027.
[52] V.A. Peters, J.J. Joesting, G.G. Freund, Il-1 receptor 2 (il-1r2) and its role in immune regulation, Brain Behav. Immun. 32 (2013) 1–8, https://doi.org/10.1016/j.bbi.2012.11.006.